Supplementary Data

From Screening to Stepwise Lithiation: Computational Insights into Fe–Porphyrin for Li-Ion Batteries

Hemjot Kaur[a], Neetu Goel[a,*]

[a] Computational and Theoretical Chemistry Group, Department of Chemistry & Centre for Advanced Studies in Chemistry, Panjab University, Chandigarh-160014, India

* Corresponding author, neetugoel@pu.ac.in

Table S1. The optimized geometries of the MPr@AM and nearest atom distance of AM with MPr.

System	Optimized Geometry	System	Optimized Geometry
MnPr@Li	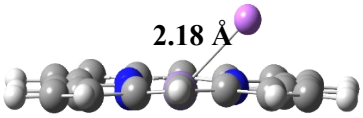	**CoPr@Li**	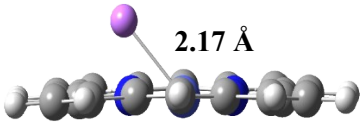
MnPr@Na	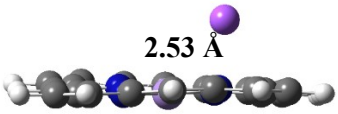	**CoPr@Na**	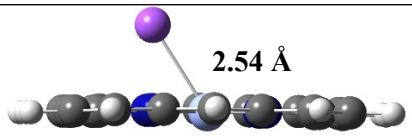
MnPr@K	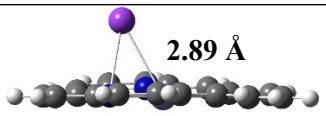	**CoPr@K**	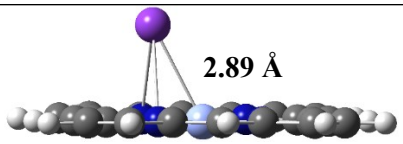
FePr@Li	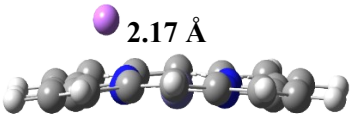	**NiPr@Li**	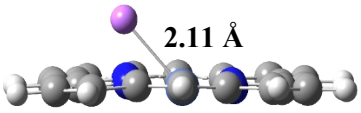
FePr@Na	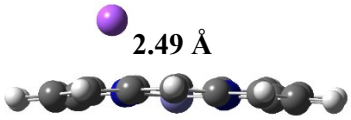	**NiPr@Na**	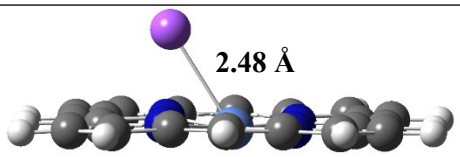
FePr@K	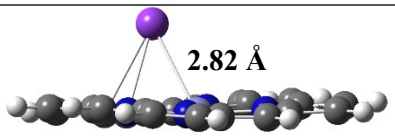	**NiPr@K**	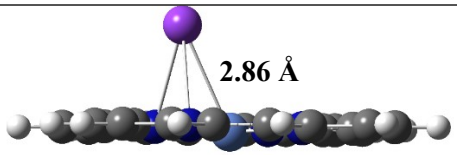

CuPr@Li	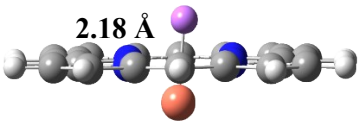	**ZnPr@Li**	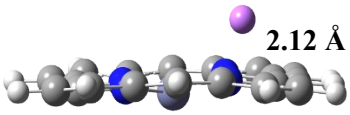
CuPr@Na	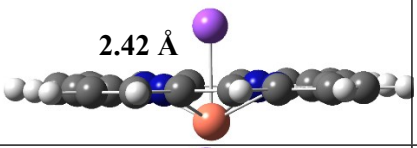	**ZnPr@Na**	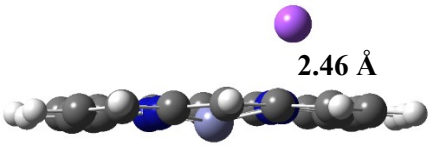
CuPr@K	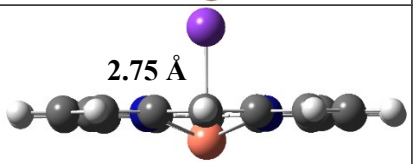	**ZnPr@K**	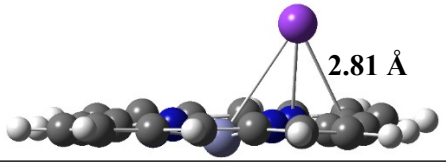

Table S2. Structural parameters for FePr@7Li and FePr@8Li, including RMSD (Å), Fe-N bond length *d* (Å), and dihedral angles ϕ (°). Atom labeling follows the optimized geometry shown in Fig. 1A.

Structural parameter	**FePr@7Li**	**FePr@8Li**
Geometry	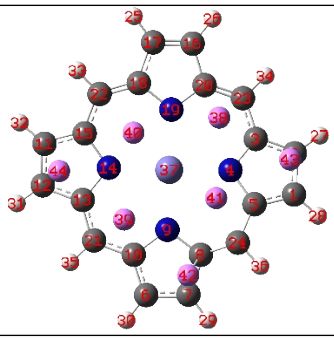	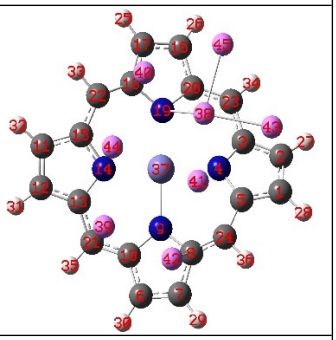
RMSD*	Reference	0.3598
$d_{Fe\text{-}N}$	2.03	1.99
$\Phi(Fe_{37}N_4C_3C_{23})$	21.74	26.96
$\Phi(N_4C_3C_{23}N_{19})$	−6.17	−9.78
$\Phi(N_4C_5C_{24}N_9)$	21.96	16.19

*The root-mean-square deviation (RMSD) was calculated according to the following expression [1]:

$$\sqrt{\frac{1}{N}\sum_{i}^{N}[(x_i - x_i^{'})^2 + (y_i - y_i^{'})^2 + (z_i - z_i^{'})^2]}$$

where N is the number of atoms, and (x_i, y_i, z_i) and (x_i', y_i', z_i') are the Cartesian coordinates of atom i in the compared (FePr@8Li) and reference (FePr@7Li) structures, respectively. Prior to RMSD evaluation, optimal least-squares superposition was performed using the Kabsch algorithm [2] to remove rotational and translational contributions. FePr@7Li was taken as the reference structure. The following figure shows the superposition of optimized FePr@7Li (reference) and FePr@8Li structures after optimal least-squares alignment using the Kabsch algorithm. The FePr@7Li reference geometry is shown with sky-blue bonds and blue atoms, while the FePr@8Li structure is shown with orange bonds and pink atoms. Overall rotational and translational motions have been removed prior to comparison. Green connectors highlight the atomic deviations between the two structures, clearly illustrating the lithiation-induced geometric distortion upon adsorption of the eighth Li atom.

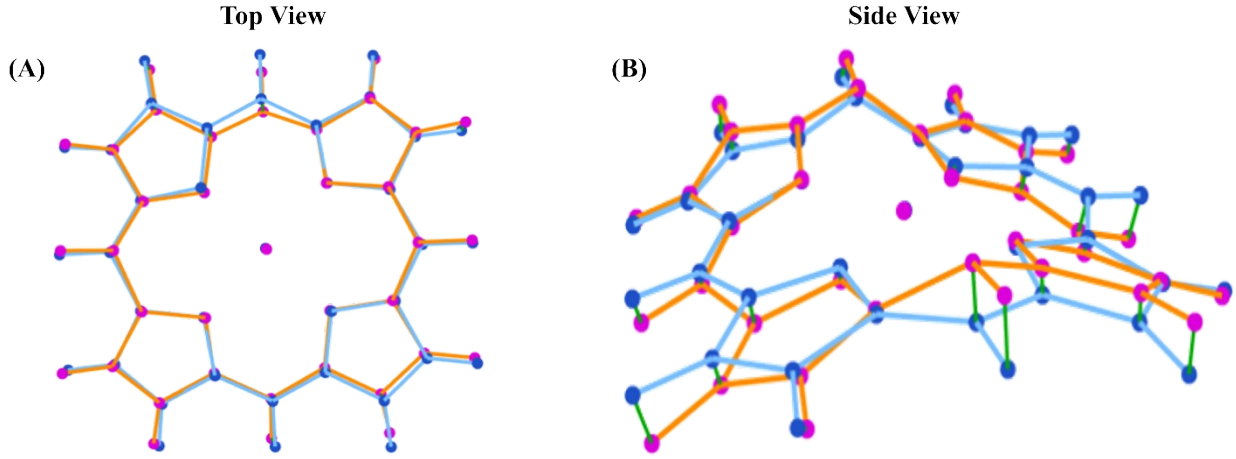

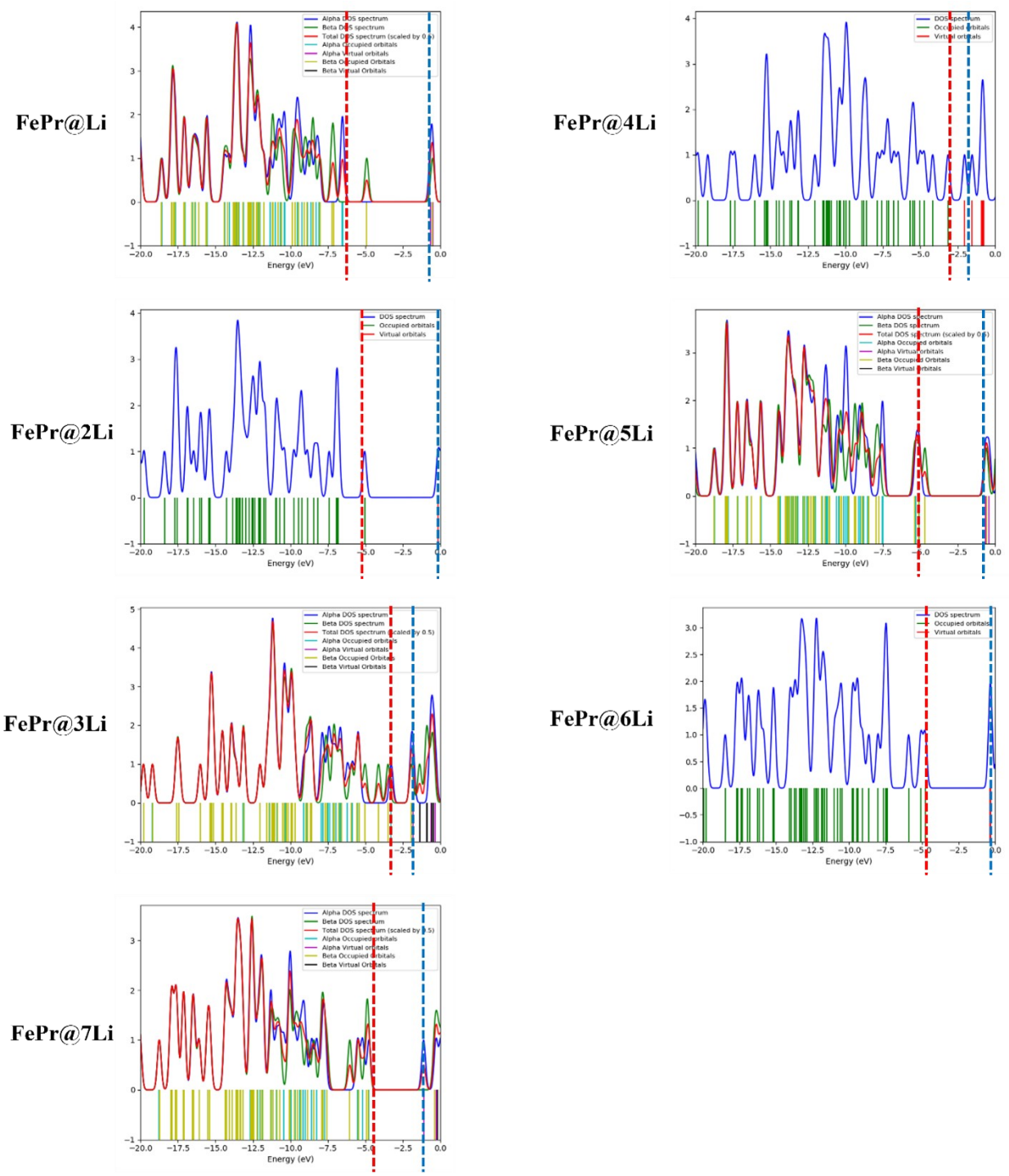

Fig. S1. The DOS plots of the FePr@nLi. Vertical dashed lines denote the HOMO (red) and LUMO (blue) values. The band gap corresponds to the zero-DOS region between these levels, apparent DOS intensity near the gap edges arises from Gaussian broadening of discrete molecular orbitals.

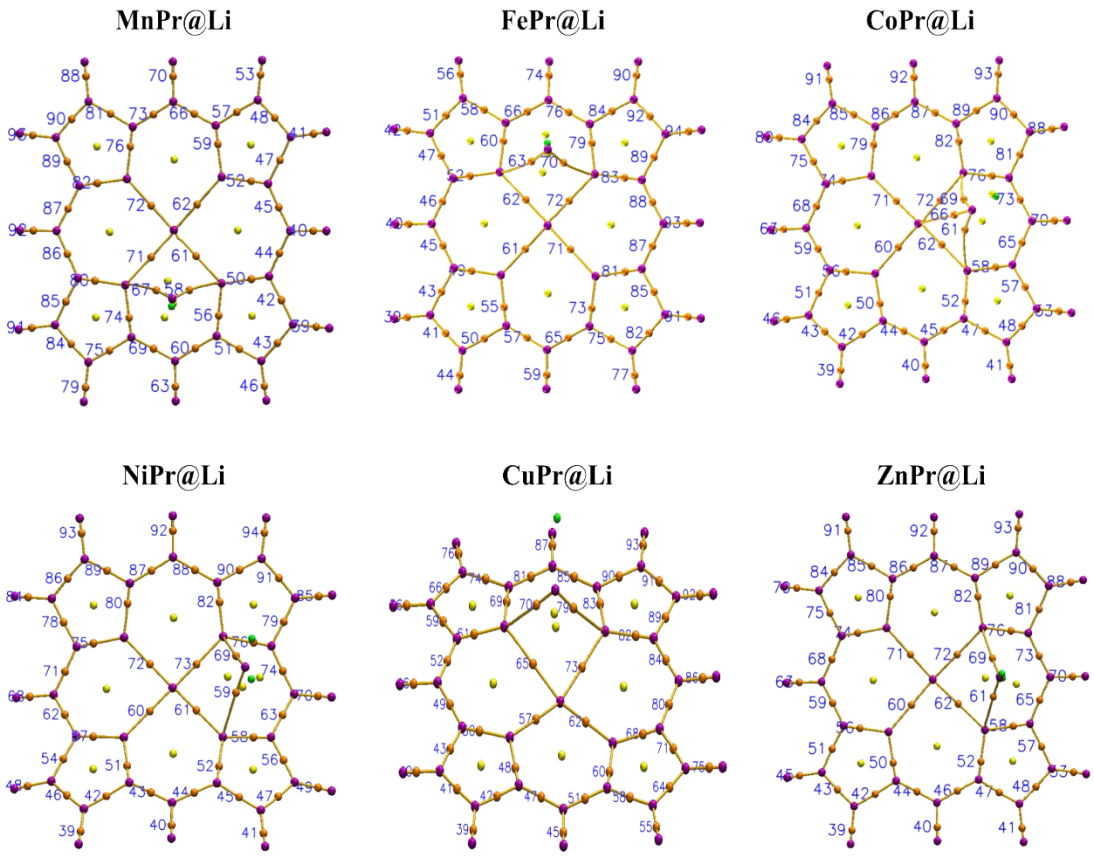

Fig. S2. QTAIM bond paths and BCPs for Li–MPr interactions (labelled BCPs correspond to Table 2).

Table S3. Selected NBO second-order perturbation (donor → acceptor) analysis showing stabilization energies E(2) (kcal mol^{-1}), donor-acceptor energy differences E(j)-E(i) (a.u.), and Fock matrix element F(i,j) (a.u.) for MPr@Li and successive lithiation.

System	Donor (i)	Acceptor (j)	E(2)	E(j) – E(i)	F(i,j)
MnPr@Li	BD*(2) C17–C18	BD*(2) C15–C22	389.88	0.01	0.093
FePr@Li	BD*(2) C3–N4	BD*(2) C20–C23	140.32	0.06	0.137
CoPr@Li	BD*(2) C8–C24	BD*(2) C6–C7	222.60	0.01	0.077
NiPr@Li	BD*(2) C3–N4	BD*(2) C20–C23	120.12	0.08	0.151
CuPr@Li	BD*(2) C3–N4	BD*(2) C20–C23	189.83	0.05	0.118
ZnPr@Li	LP(1) C15	BD*(2) C13–N14	67.33	0.10	0.110
FePr@2Li	BD*(2) C6–C10	BD*(2) C7–C8	339.57	0.02	0.096
FePr@3Li	LP(1) Li40	LP*(1) Li39	231.86	0.01	0.096
FePr@4Li	LP(1) C18	BD*(2) N19–C20	128.84	0.12	0.112
FePr@5Li	LP*(1) Li38	LP*(1) Li40	196.21	0.01	0.095
FePr@6Li	BD*(2) C2–C3	BD*(2) C20–C23	214.18	0.02	0.084
FePr@7Li	LP(1) C22	BD*(2) C18–N19	191.78	0.13	0.197

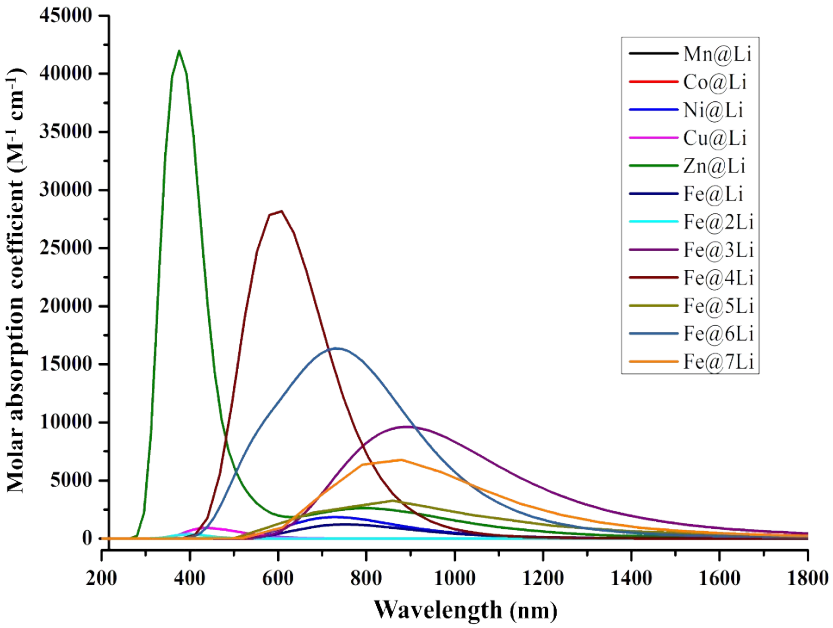

Fig. S3. Simulated UV–Vis spectra for Li-MPr systems in IEF-PCM (acetonitrile).

Table S4. TD-DFT vertical excitation energies (E, eV), corresponding wavelengths (λ, nm), oscillator strengths (f) and main orbital contributions (%) for MPr@Li systems in gas phase and with solvent (IEF-PCM, acetonitrile).

	Without Solvent				With Solvent			
System	**E**	**λ**	**f**	**Major composition**	**E**	**λ**	**f**	**Major composition**
MnPr@Li	1.571	789.07	0.0012	H → L (44.08%), H → L+3 (30.35%)	2.827	438.51	0.0305	H-1 → L (59.28%), H-2 → L+1 (37.08%)
CoPr@Li	2.391	518.53	0.0147	H → L+1 (34.22%), H-1 → L (23.17%)	1.375	901.69	0.0001	H-2 → L+1 (86.12%), H → L (6.67%)
NiPr@Li	1.511	820.39	0.0052	H → L+3 (32.09%)	1.688	734.42	0.0379	H → L (33.29%), H-1 → L+1 (20.89%)
CuPr@Li	1.460	848.98	0.0003	H → L (78.49%), H → L+1 (19.93%)	2.940	421.64	0.0151	H-1 → L (4.38%), H-4 → L+1 (10.24%)
ZnPr@Li	3.231	383.71	0.4188	H → L+2 (87.47%), H-2 → L (26.42%)	3.110	398.63	0.7288	H → L+1 (88.38%), H-1 → L (44.98%)
FePr@Li	1.480	838.04	0.0004	H → L (20.90%), H → L+1 (8.16%)	1.647	752.80	0.0302	H → L+1 (27.97%), H-1 → L (21.09%)
FePr@2Li	1.843	672.60	0.0042	H → L+2 (75.20%), H-1 → L (11.45%)	3.201	387.34	0.0062	H → L+2 (85.94%), H → L+3 (3.07%)
FePr@3Li	1.274	973.34	0.0007	H-1 → L (97.87%), H → L (11.42%)	1.392	890.69	0.2368	H-1 → L (2.61%)
FePr@4Li	1.918	646.44	0.1705	H → L+3	1.938	639.92	0.3901	H → L+1 (93.11%)

				(95.34%)				
FePr@5Li	1.466	845.81	0.0578	H-1 → L+2 (10.12%), H-1 → L+2 (10.12%)	1.529	810.90	0.0242	H-2 → L (18.22%), H-1 → L (17.99%)
FePr@6Li	1.529	811.07	0.0223	H → L+1 (43.19%), H-1 → L (25.27%)	1.628	761.63	0.3508	H → L (92.93%)
FePr@7Li	1.285	964.87	0.0101	H-2 → L (87.06%), H-1 → L (17.76%)	1.361	911.17	0.0565	H-1 → L+1 (82.34%), H → L+1 (49.71%)

References:

1. Xie J, Shi H, Shen C, Huan L, He M, Chen M. Heteroatom-bridged pillar [4] quinone: evolutionary active cathode material for lithium-ion battery using density functional theory. Journal of Chemical Sciences. 2021 Mar;133(1):2.
2. Kabsch W. A discussion of the solution for the best rotation to relate two sets of vectors. Foundations of Crystallography. 1978 Sep 1;34(5):827-8.